The amyloid-β$_{1-42}$-oligomer interacting peptide D-AIP possesses favorable biostability, pharmacokinetics, and brain region distribution

Adeola Shobo[1] , Nicholas James[2] , Daniel Dai[3] , Alexander Röntgen[1,4] , Corbin Black[3] , Jean-Robert Kwizera[1],
Mark A. Hancock[1] , Khanh Huy Bui[3] , and Gerhard Multhaup[1,2,*]
From the [1]Department of Pharmacology and Therapeutics, [2]Integrated Program in Neuroscience, and [3]Strathcona Anatomy Dentistry Building, McGill University, Montreal, Quebec, Canada; [4]Institute of Biochemistry, University of Cologne, Cologne, Germany

Edited by Paul Fraser

We have previously developed a unique 8-amino acid Aβ42 oligomer-Interacting Peptide (AIP) as a novel anti-amyloid strategy for the treatment of Alzheimer's disease. Our lead candidate has successfully progressed from test tubes (*i.e.*, *in vitro* characterization of protease-resistant D-AIP) to transgenic flies (*i.e.*, *in vivo* rescue of human Aβ42-mediated toxicity *via* D-AIP-supplemented food). In the present study, we examined D-AIP in terms of its stability in multiple biological matrices (*i.e.*, *ex-vivo* mouse plasma, whole blood, and liver S9 fractions) using MALDI mass spectrometry, pharmacokinetics using a rapid and sensitive LC-MS method, and blood brain barrier (BBB) penetrance in WT C57LB/6 mice. D-AIP was found to be relatively stable over 3 h at 37 °C in all matrices tested. Finally, label-free MALDI imaging showed that orally administered D-AIP can readily penetrate the intact BBB in both male and female WT mice. Based upon the favorable stability, pharmacokinetics, and BBB penetration outcomes for orally administered D-AIP in WT mice, we then examined the effect of D-AIP on amyloid "seeding" *in vitro* (*i.e.*, freshly monomerized *versus* preaggregated Aβ42). Complementary biophysical assays (ThT, TEM, and MALDI-TOF MS) showed that D-AIP can directly interact with synthetic Aβ42 aggregates to disrupt primary and/or secondary seeding events. Taken together, the unique mechanistic and desired therapeutic potential of our lead D-AIP candidate warrants further investigation, that is, testing of D-AIP efficacy on the altered amyloid/tau pathology in transgenic mouse models of Alzheimer's disease.

Amyloid-beta (Aβ) peptides are central to the pathogenesis of Alzheimer disease (AD), based upon the discovery of protective and risk variants in the gene encoding the amyloid precursor protein (APP) and other genes of the amyloid response pathways (1, 2). Aβ peptides of varying length are produced by the sequential, proteolytic processing of APP by the beta- and gamma-secretases in the amyloidogenic pathway (3, 4). Notably, the 40-amino acid peptide (Aβ40) is most abundant, whereas the 42-amino acid peptide (Aβ42) is most prone to aggregate into amyloid oligomers and the main component of senile plaques (5). *In vitro* and *in vivo* studies have shown that soluble Aβ42 oligomers are highly toxic to neuronal cells (*i.e.*, impair synaptic function) and their conversion and accumulation into fibrils is associated with progressive neuronal dysfunction and cognitive decline (6–8). Studies investigating the structural and biochemical properties of Aβ and tau have advanced our understanding of AD and the associated pathology at the molecular level (9). In particular, the pathological cascade of sporadic AD appears to be triggered by impaired Aβ degradation and clearance (10). Compared with the gold standard Aβ40/42 peptide ratio (*i.e.*, indicator of amyloid deposition), which is currently used to assess AD progression before cognitive symptoms appear (11), other Aβ peptides and ratios (*e.g.*, Aβ34 and Aβ34/Aβ42, respectively) are emerging as earlier markers of reduced amyloid clearance in presymptomatic AD (12).

Multimeric, Aβ42-containing amyloid seeds are believed to serve as starter molecules of the amyloid cascade (13), thereby promoting the formation of plaque deposits in various areas of the brain (2, 9, 14). These so called pathogenic "seeds" supposedly form important anchor points that favor an elongation process that assembles monomeric Aβ into larger oligomers (15). As a putative therapeutic target, pathogenic Aβ seeds already exist throughout the lag phase of protein aggregation in the brain when the aggregation of minute amounts of Aβ peptides presumably marks the beginning of AD (16). To specifically target these seeds during the preclinical phase of AD as a novel anti-amyloid strategy, we have been developing a unique 8-amino acid Aβ42-oligomer Interacting Peptide (AIP), a nonamidated version of the RGTFEGKF peptide (17). We previously showed that AIP could render a population of low-order Aβ42 oligomers nontoxic, thus suppressing the formation of mature fibrils (18, 19). The peptide was more stable against proteolysis when synthesized using D-amino acids (*i.e.*, D-AIP), yet retained the same functional properties as its original L-amino acid counterpart (*i.e.*, L-AIP) including its direct interaction with the early Aβ42 aggregates (18).

Subsequently, our longitudinal *in vivo* study (19) used a *Drosophila melanogaster* model, expressing human Aβ42 in the eyes of the flies, to successfully demonstrate that (i) D-AIP could penetrate the blood brain barrier (BBB) and prevent Aβ42-mediated toxicity in the transgenic flies and (ii) the continuous dosing with D-AIP had no adverse effect on the survival rates or locomotion of WT or transgenic flies.

In the present study, we investigated the *ex-vivo* stability of D-AIP as a nontoxic drug candidate in biological matrices including mouse plasma, whole blood, and liver S9 fractions. Progressing from short-term (0.5–24 h at 10, 30, or 100 mg/kg) to long-term administration (30 days at 10 mg/ml), we also determined the *in vivo* pharmacokinetic (PK) properties of D-AIP by assessing the area under the curve (AUC), maximum concentration reached (C_{max}), time at which maximum concentration is reached (T_{max}), elimination rate constant (λz), elimination half-life ($t_{1/2}$), apparent total clearance from plasma after oral administration (CL/F), apparent volume of distribution (V_d), and mean residence time (MRT). After the short- or long-term oral doses of D-AIP were administered to male and female WT (C57BL6) mice, D-AIP was quantified in the plasma and brain homogenates at the designated time points by LC-MS. Using MALDI-mass spectrometry imaging (MSI), the spatial localization of label-free D-AIP was detected in sagittal sections of the WT mouse brains to verify that D-AIP could readily penetrate the intact BBB. Regarding the primary and secondary nucleation events that promote amyloid "seeding", we also used complementary biophysical techniques (thioflavin T (ThT) aggregation and transmission electron microscopy (TEM) assays) to monitor the aggregation state of synthetic Aβ42 peptides (freshly monomerized *versus* preaggregated) in the absence and presence of D-AIP. Collectively, our present *ex-vivo*, *in vivo*, and biophysical data indicate that D-AIP possesses favorable attributes that may attenuate amyloid and/or tau pathology in follow-up studies involving the transgenic mouse models of AD.

Results

Ex-vivo *stability of D-AIP in mouse plasma, whole blood, and liver S9 fractions*

Previously, we have shown that D-AIP, in contrast to L-AIP, was stable toward proteolytic degradation in supplemented fly food and *D. melanogaster* for up to 28 days (19). Here, we investigated the stability of D-AIP in mouse plasma, blood, and liver S9 fractions to determine its metabolic resistance toward proteases and enzymatic activities in these matrices. For example, to mimic oral administration events and assess the first-pass effect of the liver on D-AIP, we incubated liver S9 fractions with D-AIP.

The stability of D-AIP was evaluated in pooled samples taken from male and female WT (C57BL6) mice after D-AIP was spiked and incubated at 37 °C for 1, 3 or 24 h in all three biological matrices. The multi-time point aliquots were biochemically processed and analyzed by MALDI-TOF mass spectrometry. The relative peak intensities for control-only PBS, protease-resistant D-AIP, protease-sensitive L-AIP, and a scrambled version of D-AIP (sD-AIP) were compared across all MALDI-TOF spectra (Figs. 1, *A–C* and S1, *A–C*). The stability of D-AIP at 37 °C over 24 h was greatest in whole blood followed by plasma then liver S9 fractions. In contrast, L-AIP was rapidly degraded in mouse whole blood as indicated by the significantly reduced signal intensities at the earlier 1 and 3 h time points, and no L-AIP signal remained after 24 h at 37 °C in mouse liver S9 fractions. Signals for both D-AIP and its sD-AIP decreased only two-fold over 24 h at 37 °C in mouse whole blood, whereas larger three-fold or four-fold decreases for D-AIP and sD-AIP were observed under identical conditions in mouse liver S9 fractions. Overall, a general trend in reduced peak intensities was observed for all three peptides at the 3 h time point, indicating biodegradability when incubated in the liver S9 fractions as shown in Fig. S1*C*. Generally, D-AIP appeared to be very stable in plasma and blood matrices, which was anticipated because D-amino acid peptides are known to be resistant against proteolysis (20). Based upon the desirable *ex-vivo* stability of D-AIP in the present study (*i.e.*, long-term (24 h) exposure to blood and liver enzymes at 37 °C), D-AIP likely represents an orally administrable compound if it is similarly stable *in vivo*.

Plasma pharmacokinetics of D-AIP in C57BL/6 mice

To investigate the PK properties of D-AIP, we performed a short-term, dose ranging study with C57BL/6 mice after single oral dosing at 10, 30, or 100 mg/kg D-AIP. To quantify D-AIP in the plasma obtained from the dosed male and female 7 to 9 weeks old C57BL/6 mice (n = 3), we developed a sensitive and rapid biochemical LC-MS method (see Experimental procedures) to help determine the final PK parameters (Table 1). At 24 h postadministration, the AUC_{0-t} values in females were 261.11, 643.10, and 1928.30 ng h ml^{-1}, whereas the AUC_{0-t} values in males were 270.86, 825.73, and 2041.98 ng h ml^{-1} after the single oral doses at 10, 30, or 100 mg/kg D-AIP, respectively. These doses yielded maximum plasma drug concentrations (C_{max}) in females of 48.41, 76.57, and 372.25 ng ml^{-1} and in males of 41.52, 123.53, and 332.51 ng ml^{-1}, respectively.

C_{max} were reached in female plasma after 2 h with 10 and 30 mg/kg doses and after 0.5 h for the 100 mg/kg dose. T_{max} in males was reached after 2 h for the 10 mg/kg dose and 0.5 h for higher doses, that is, 30 and 100 mg/kg. The elimination rate constant (λz) in the females were 0.06, 0.10, and 0.21 h^{-1}, whereas the rates were determined to be 0.15, 0.21, and 0.24 h^{-1} in males at the 10, 30, and 100 mg/kg doses, respectively. The $t_{1/2}$ in the females were 11.92, 6.70, and 3.34 h, whereas the values were 4.56, 3.23, and 2.91 h in males, respectively. The CL/F of the D-AIP from plasma after respective oral doses given to female mice were 30.04, 42.02, and 51.54 l h^{-1}, whereas the corresponding values for males were 35.81, 36.02, and 48.79 l h^{-1}. V_d values were 516.64, 406.00, and 248.74 l in females after administration, whereas it reached 235.34, 167.76, and 204.84 l in the males, respectively. The values for the MRT in the female mice were 14.34, 9.57, and 4.47 h, however MRT values in males reached 6.42, 5.85, and 5.29 h
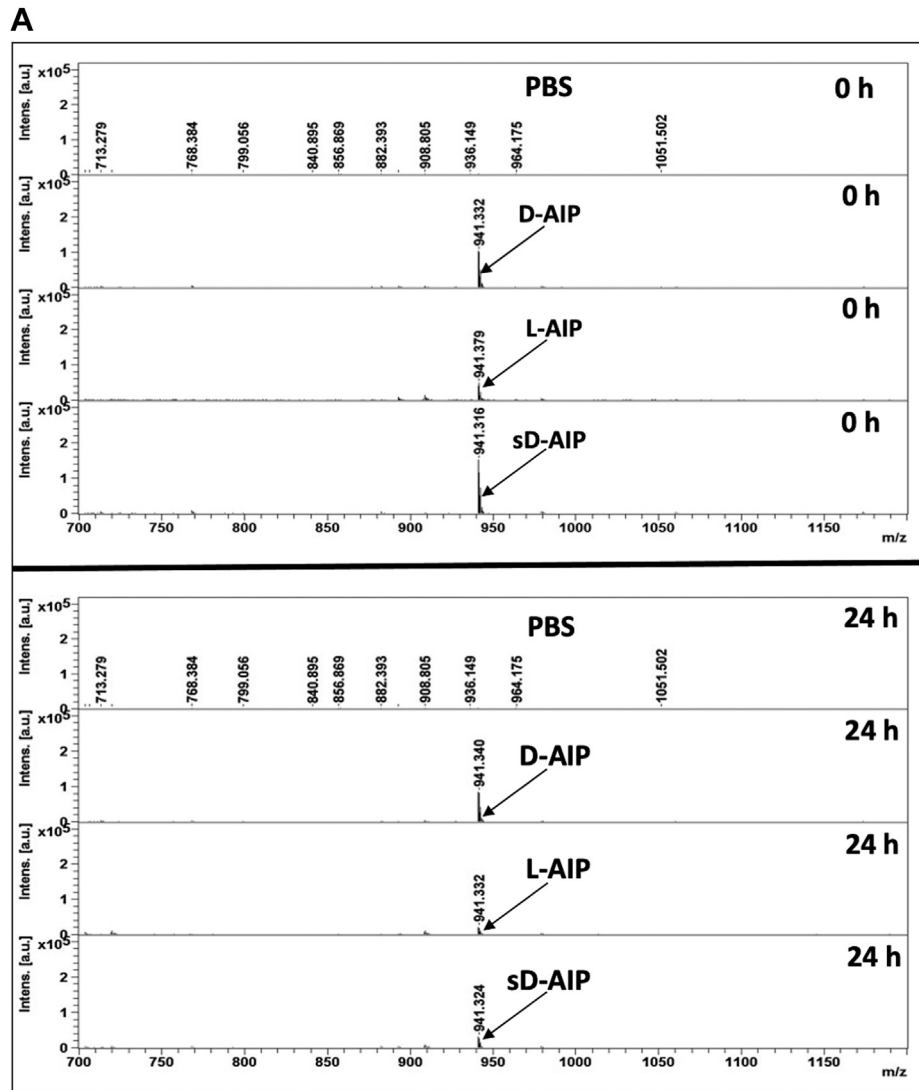
Figure 1A. *Ex-vivo* stability of AIP (941 *m/z*) in mouse plasma. PBS, D-AIP (RGTFEGKF), L-AIP (RGTFEGKF), or sD-AIP (EFRKFTGG) were spiked into mouse plasma and incubated at 37 °C for 0 h (*upper panel*) or 24 h (*lower panel*). MALDI-TOF spectra showed that D-AIP was relatively stable in mouse plasma at 37 °C until 24 h, whereas the relative intensity of L-AIP diminished to about a third of the initial signal intensity under identical conditions. AIP, Aβ42-oligomer interacting peptide; D-AIP, AIP (RGTFEGKF) synthesized using D-amino acids; L-AIP, AIP (RGTFEGKF) synthesized using L-amino acids; sD-AIP, scrambled version of D-AIP.

after the respective doses. The D-AIP concentration-time profiles in plasma show the absorption of D-AIP in the female (Fig. 2A) and male (Fig. 2B) C57BL/6 mice. The plasma concentrations of D-AIP declined and reached baseline levels after 24 h in both sexes and at all doses administered, thus suggesting that D-AIP was distributed to tissues and eliminated from the peripheral system over time. The significantly higher values observed for the half-life, V_d and MRT in females at lower doses is sex specific, whereas the overall values at 100 mg/kg were grossly the same for both sexes. At the highest dose, 100 mg/kg, D-AIP achieved a steady state, which seemingly triggered the elimination from the body, reduced its MRT, plasma half-life and V_d and thus attenuated the differences observed between sexes at lower concentrations. The D-AIP plasma profiles for all treated mice were similar in shape with very few exceptions. Possible differences could be related to physiological factors including sex-related drug metabolism.

In this study, all single doses of orally administered D-AIP were well-tolerated with no detectable vital signs of abnormalities before or after the animals were terminated. When the calculated AUC values (*i.e.*, indicator of total systemic exposure to D-AIP at each dose) were plotted as a function of the doses, profiles for the male and female mice demonstrated a similarly linear dependence (Fig. S2).

Brain concentration profiles of D-AIP in C57BL/6 mice

The BBB is a structural and functional semipermeable border of endothelial cells between the interstitial fluid of the brain and the blood. To evaluate the propensity of D-AIP to cross the BBB, we determined the concentration of D-AIP in mouse brains after the single oral dose treatments (10, 30, or 100 mg/kg) in female and male 7 to 9 weeks old C57BL/6 mice (n = 3). Across the different time points, D-AIP concentrations
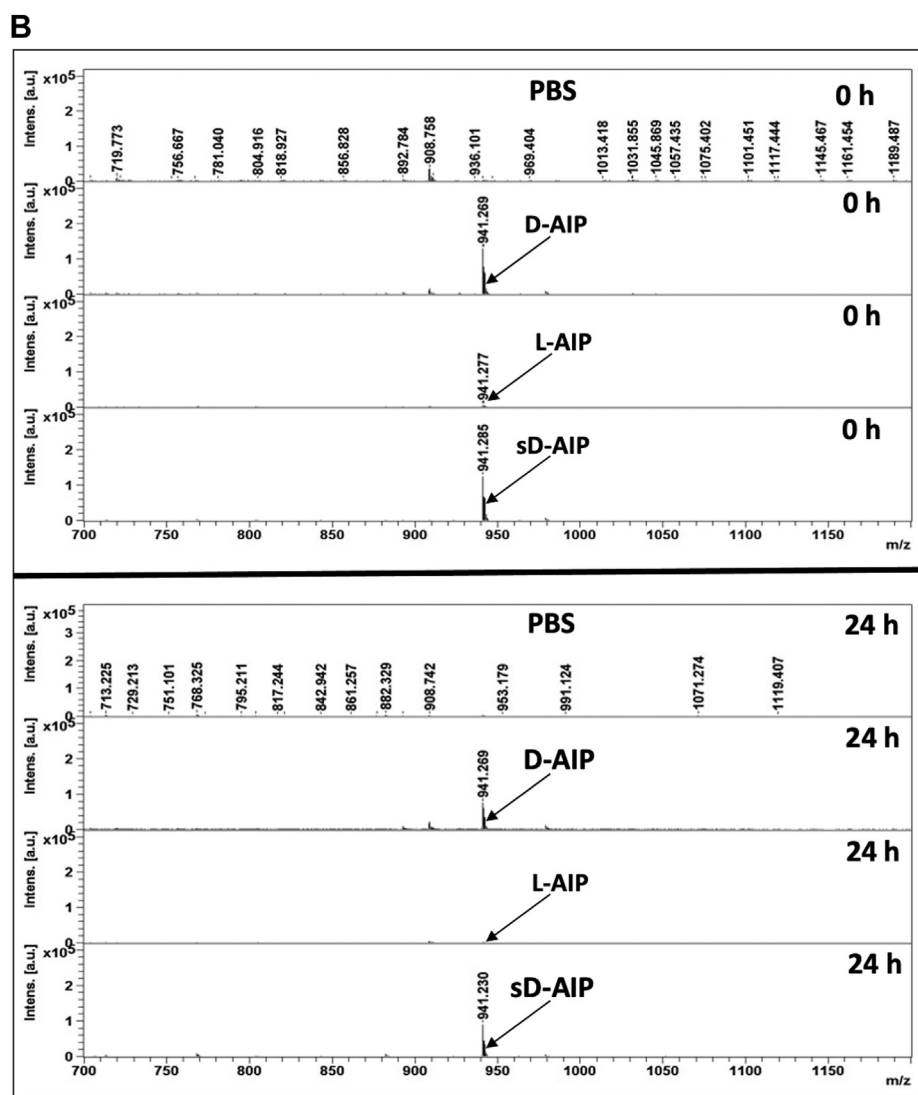
⬡ASBMB

J. Biol. Chem. (2022) 298(1) 101483 **3**

Figure 1B. *Ex-vivo* stability of AIP (941 *m/z*) in whole blood. PBS, D-AIP (RGTFEGKF), L-AIP (RGTFEGKF), or sD-AIP (EFRKFTGG) were spiked into mouse whole blood and incubated at 37 °C for 0 h (*upper panel*) or 24 h (*lower panel*). MALDI-TOF spectra showed that D-AIP was relatively stable in mouse blood at 37 °C until 24 h, whereas the relative intensity of L-AIP was no longer detectable under identical conditions. AIP, Aβ42-oligomer interacting peptide; D-AIP, AIP (RGTFEGKF) synthesized using D-amino acids; L-AIP, AIP (RGTFEGKF) synthesized using L-amino acids; sD-AIP, scrambled version of D-AIP.

were determined in the prepared brain homogenates using our sensitive LC-MS method. The D-AIP brain concentrations reached their maximal values of 28.91 ng/g at 4 h, 136.29 ng/g at 2 h, and 707.95 ng/g at 2 h in female mice after the 10, 30, or 100 mg/kg doses, respectively (Fig. 3*A*). The male mice reached peak concentrations of 133.15 ng/g, 262.00 ng/g, and 509.24 ng/g D-AIP after the respective doses at 4 h, 2 h, and 0.5 h (Fig. 3*B*). At the highest 100 mg/kg dose administered, the concentration profiles revealed that the transport of D-AIP to the brain was faster in male mice (within 0.5–2 h), but its subsequent elimination was gradual over 3.5 h (*i.e.*, concentration of 166.57 ng/g at 4 h time point). Surprisingly, D-AIP levels rapidly decreased within only 2 h in female mice (*i.e.*, concentration of 16.67 ng/g at 4 h time point). The more efficient elimination of D-AIP from the brain of female mice likely relates to sex-based differences in body physiology, which were also noted in plasma concentration profiles

(Fig. 2). Overall, the present data indicate that D-AIP peptides enter and exit the CNS of mice of both sexes, likely by an uncharacterized transport system(s) involving capillary endothelial cells of the neurovascular unit.

Brain region distribution of D-AIP in C57BL/6 mice

To complement our quantitative LC-MS results, we also examined the relative abundance and spatial distribution of D-AIP uptake in sagittal brain sections using MALDI-MSI. Female and male C57BL/6 mice treated with a single oral dose of PBS (control) or D-AIP (10 mg/kg) were sacrificed after 4 h, and the brain sections were prepared for the MALDI tissue imaging. Once the data was acquired, the appropriate mass filter (D-AIP = 941 *m/z*) was applied to generate 'heat maps' depicting the relative intensity (low to high: blue to white) and spatial localization of D-AIP within the sagittal brain sections
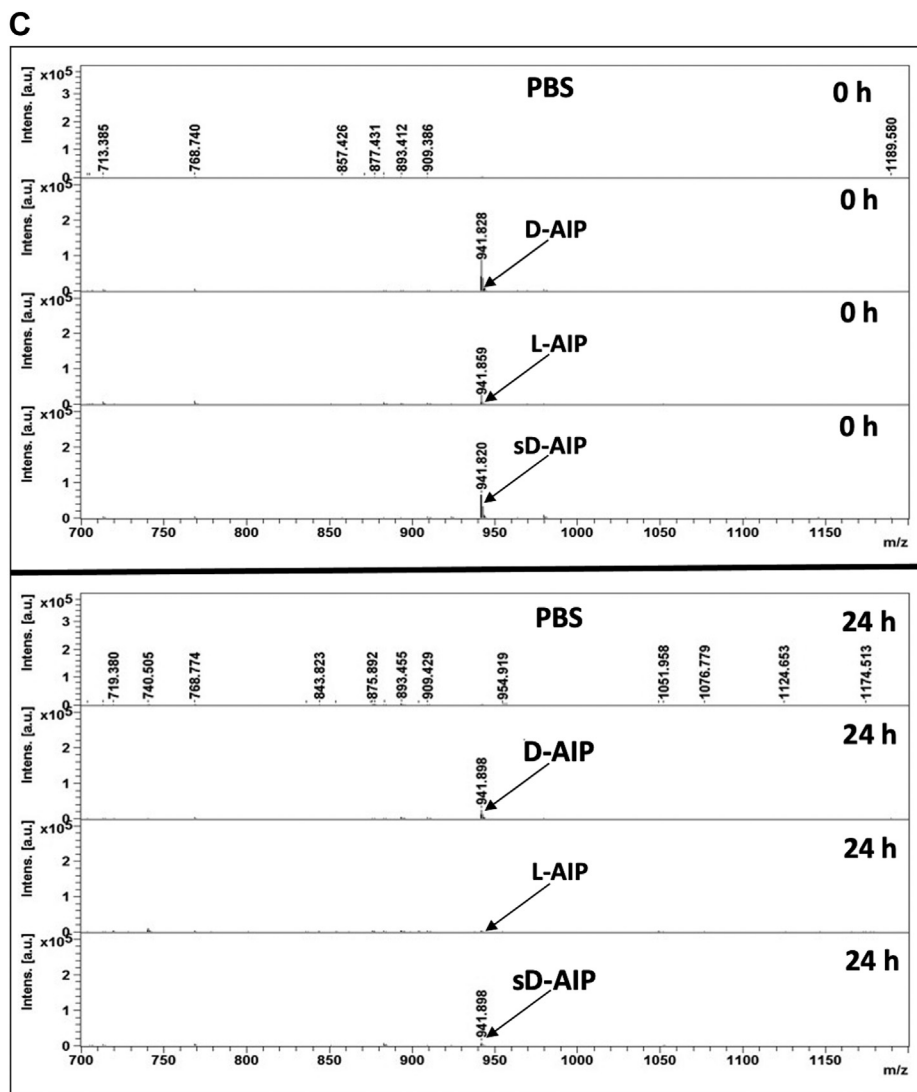
Figure 1C. *Ex-vivo* stability of AIP (941 *m/z*) in mouse liver S9 fractions. PBS, D-AIP (RGTFEGKF), L-AIP (RGTFEGKF), or sD-AIP (EFRKFTGG) were spiked into mouse liver S9 fraction and incubated at 37 °C for 0 h (*upper panel*) or 24 h (*lower panel*). MALDI-TOF spectra showed that D-AIP was relatively stable in mouse liver S9-fraction at 37 °C until 24 h, whereas L-AIP was degraded under identical conditions when its peak (941 *m/z*) was no longer detected. AIP, Aβ42-oligomer interacting peptide; D-AIP, AIP (RGTFEGKF) synthesized using D-amino acids; L-AIP, AIP (RGTFEGKF) synthesized using L-amino acids; sD-AIP, scrambled version of D-AIP.

at 50 μm resolution. For both female and male WT mice (*i.e.*, intact BBB), the representative MALDI-MSI results (Fig. 4) showed that there was significant D-AIP distribution (*i.e.*, intense green to pink colored heat map regions) along the cortex to the hippocampus and thalamus structures. Between the sexes, female brain sections exhibited higher D-AIP

Table 1

Pharmacokinetic parameters of D-AIP in plasma

Gender	Female	Male	Female	Male	Female	Male
Dose (mg/kg)	10	10	30	30	100	100
Pharmacokinetic parameters						
AUC_{0-t} (ng h ml^{-1})	261.11	270.86	643.10	825.73	1928.30	2041.98
AUC_{0-inf} (ng h ml^{-1})	332.92	279.27	713.88	832.96	1940.09	2049.79
C_{max} (ng ml^{-1})	48.41	41.52	76.57	123.53	372.25	332.51
T_{max} (h)	2.00	2.00	2.00	0.50	0.50	0.50
λ_z (h^{-1})	0.06	0.15	0.10	0.21	0.21	0.24
$T_{1/2}$ (h)	11.92	4.56	6.70	3.23	3.34	2.91
CL/F (l h^{-1})	30.04	35.81	42.02	36.02	51.54	48.79
V_d/F (l)	516.64	235.34	406.00	167.76	248.74	204.84
MRT (h)	14.37	6.42	9.57	5.85	4.47	5.29

Values are obtained from average of three animals (n = 3).
The results in the table were obtained from plasma samples of the dosed (female and male) 7 to 9 weeks old C57BL/6 mice at 10, 30, or 100 mg/kg after single oral (gavage) doses of D-AIP. Notably, in females, at lower doses are higher values for the half-life ($T_{1/2}$), volume of distribution (V_d), and mean residence time (MRT), which stabilized relatively at a higher dose in both sexes.
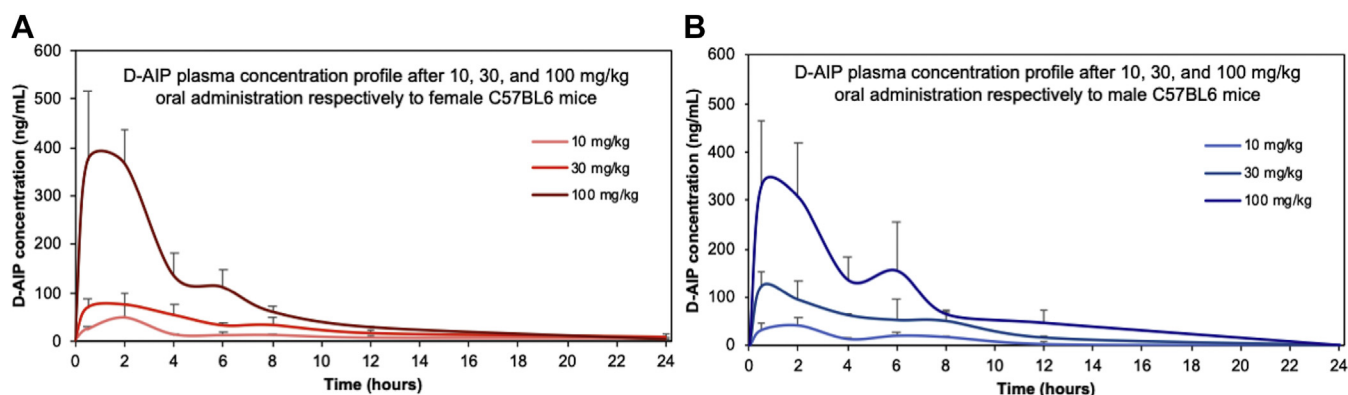
Figure 2. D-AIP concentration-time profiles in plasma. Time-dependent alterations in D-AIP concentration in plasma after a single oral (gavage) dose of 10 mg/kg, 30 mg/kg, or 100 mg/kg was administered to 7 to 9 weeks old female (*A*) in shades of *red* and male C57BL/6 mice (*B*) in shades of *blue*. At seven designated time points (0.5 h–24 h), plasma D-AIP concentrations were quantified by LC-MS after protein precipitation. The maximal plasma concentrations of D-AIP were measured at 0.5 h after the single oral dose of 100 mg/kg in both sexes: 372.25 ng/ml in females and 332.51 ng/ml in males (average of three mice (n = 3) in each group). D-AIP, AIP (RGTFEGKF) synthesized using D-amino acids.

intensity around the thalamus than the cortex or hippocampus regions; the male brain sections exhibited D-AIP intensities in the reverse order of hippocampus > cortex > thalamus. As expected, the PBS-treated mice (negative controls) exhibited low-intensity, blue-colored heat maps because there was no signal for the 941 *m/z* mass filter in the absence of D-AIP.

Long-term administration of D-AIP in C57BL/6 mice

To avoid the pain and stress commonly associated with the daily, long-term administration of therapeutic candidates to transgenic mice by oral gavage, a continuous dose of D-AIP (10 mg/ml in PBS) was provided *ad libitum* to female (n = 6) and male (n = 6) C57BL/6 mice for a period of 30 days. Delivered to the mice *via* sipper bottles, the total volume freely consumed by the female mice was more than 20% greater than the 30-days volumes consumed by the males (Fig. S3), yet the plasma concentration of D-AIP measured in the female mice (377.99 ng/ml) was lower than the male mice (428.59 ng/ml) in the end (Fig. 5*A*). Notably, the nonaccumulation of D-AIP in the plasma during the continuous 30-days dose provides strong evidence of minimal plasma protein binding and

correlates with the absence of D-AIP toxicity in 28-day old flies, as we have previously shown (19). The brain concentration of D-AIP (Fig. 5*B*) in female mice after 30 days (379.06 ng/g) was higher than the corresponding measurements in the male mice (204.32 ng/g). This finding likely reflects the previously marked difference in the volume of distribution (as noted in Table 1) and the observed variance in the total volume of D-AIP consumed by the WT mice (*i.e.*, females *versus* males). Consistent with the pharmacokinetics for our short-term D-AIP dosing, the continuous 30-days dosing provides further evidence that D-AIP can readily penetrate the intact BBB in WT mice.

Effect of D-AIP on Aβ42 aggregation and prevention of fibril growth

Building upon our previously published data (18) where we predicted that D-AIP interacts with low-order Aβ42 oligomers at a ratio of 1:4 (*i.e.*, one D-AIP molecule bound per tetramer of Aβ42 peptide), we currently tested for time- and concentration-dependent effects of D-AIP on multiple Aβ aggregation states using complementary biophysical
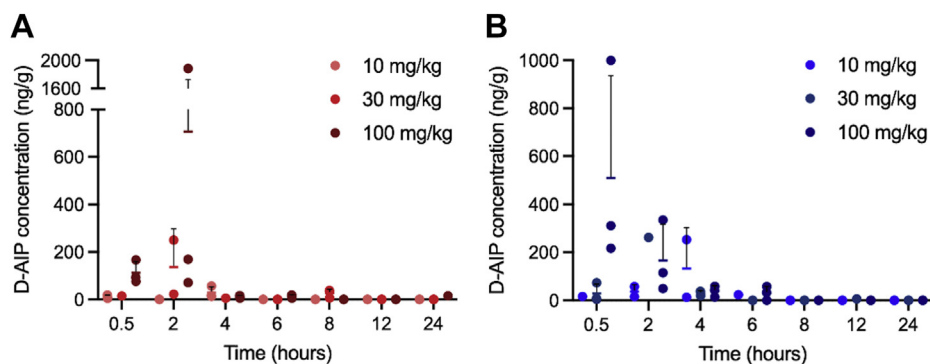

Figure 3. D-AIP concentration-time profiles in brain. Time-dependent alterations in D-AIP concentration in brain homogenates after a single oral (gavage) dose of 10, 30, or 100 mg/kg was administered to 7 to 9 weeks old female (*A*) in shades of *red* and male C57BL/6 mice (*B*) in shades of *blue*. At the designated time points, D-AIP concentrations were quantified by LC-MS (data represent average from three mice (n = 3) in each group). For all single oral doses, D-AIP crossed the BBB and reached the brain of both female- and male-treated mice. D-AIP, AIP (RGTFEGKF) synthesized using D-amino acids; BBB, blood brain barrier.
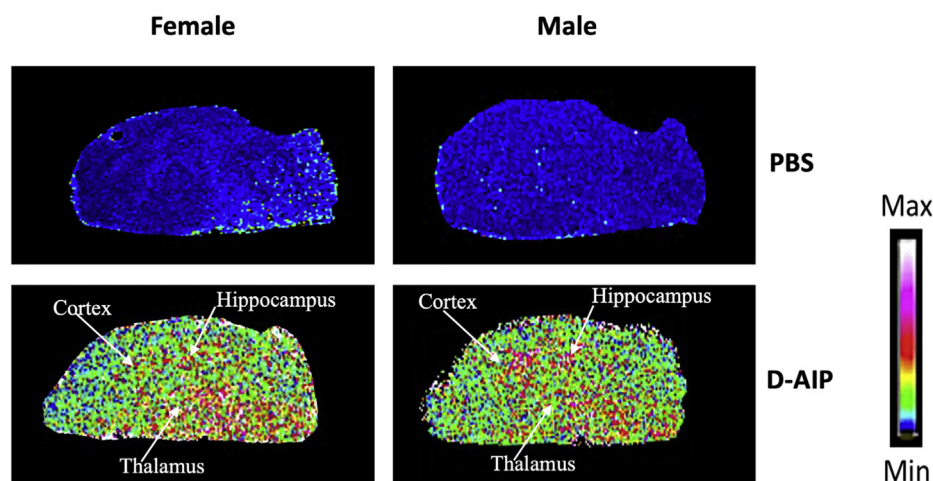
Figure 4. Brain distribution of D-AIP. MALDI-TOF-MSI analysis of label-free D-AIP in sagittal brain sections of 7 to 9 weeks old female and male C57BL/6 mice single orally (gavage) dosed with PBS or D-AIP (10 mg/kg) and sacrificed 4 h postadministration. Representative images were acquired using MALDI-TOF imaging technique, which confirms the successful entrance of D-AIP (single oral D-AIP dose of 10 mg/kg and PBS treated control) into different brain regions of treated mice (indicated by intense, *green* to *pink*-colored heat maps *versus* almost uniformly *blue*-colored background heat maps in the control). D-AIP is distributed across cortex, hippocampus, thalamus, and different other brain regions (for detected sex differences, see the text). D-AIP, AIP (RGTFEGKF) synthesized using D-amino acids.

techniques. By real-time ThT assays (Fig. 6), freshly mono-merized Aβ42 (21) or preformed aggregates (24 h) were coincubated with D-AIP for 24 h at three different D-AIP:Aβ42 ratios (*i.e.*, equimolar (1:1), four-fold (1:4), or ten-fold (1:10) molar excess of Aβ42). In the absence of D-AIP, binding of the ThT dye to Aβ42 resulted in positive fluorescence intensities at time zero which continued to further increase (Fig. 6A) and/or plateau (Fig. 6B) over 24 h or 24 to 48 h, respectively. For freshly monomerized Aβ42 in the presence of D-AIP, all three D-AIP:Aβ42 ratios considerably attenuated the primary 24-h fluorescence increases compared with control (Aβ42 only), but the 1:4 ratio appeared to be most efficient (Fig. 6A). For the preformed Aβ42 aggregates in the presence of D-AIP, all three ratios inhibited the secondary 24 to 36 h fluorescence increase (*i.e.*, fibril growth/maturation)

when compared with the Aβ42-only control (Fig. 6B); after 36 h, there was a stoichiometric and saturable interaction between ThT and amyloid fibrils, which is evident from the plateaus of the *in situ* ThT fluorescence curves.

Complementary TEM analyses (Fig. 7) cross-validated that D-AIP can inhibit the conversion of low-n Aβ42 oligomers into mature fibrils (*i.e.*, Fig. 7, *A* and *B* matches previous 1:20 result by Barucker *et al.* (18)). Specifically, long and branch-like fibrils were observed after freshly monomerized Aβ42 was incubated for 24 h in the absence of D-AIP (Fig. 7A), as compared with the short and sparse strand-like structures that resulted when fibril maturation was attenuated in the presence of D-AIP (Fig. 7B). We also observed that a similar 1:20 D-AIP ratio can also inhibit the conversion of preformed Aβ42 aggregates into densely packed mature fibrils (*i.e.*, compare Fig. 7, *C* and *D*). After monomerized Aβ42 was incubated for 24 h, fibril widths in the presence of D-AIP were enlarged (*i.e.*, 18 nm compared with 10 nm; Fig. 7E); after preformed Aβ42 aggregates were incubated for 24 h, there was no significant difference between the resulting fibril widths at 48 h in the absence or presence of D-AIP (*i.e.*, approximately 8 nm). After co-incubation for 24 h, we also used MALDI-TOF mass spectrometry (Fig. 7, *F–I*) to detect the direct binding of D-AIP to a variety of Aβ42 oligomers. Thus, the inhibitory effect of D-AIP on early aggregation steps likely reflects its direct binding to Aβ42 tetramers and pentamers and hexamers.
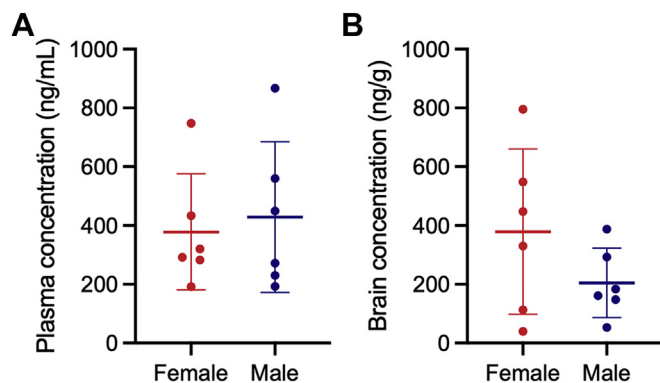

Figure 5. Plasma and brain concentration of D-AIP after long-term administration. Plasma and brain concentration of D-AIP (10 mg/ml) after a 30-days oral (sipper bottle) administration to 8-weeks old female and male C57BL/6 mice. Plasma concentration (*A*) in female mice (in *red*) was slightly lower than male mice (in *blue*) while in comparison with the brain concentration (*B*), the male (in *blue*) had a lower brain concentration than the female (in *red*). The marked brain concentration difference might be because of the previously higher values in the volume of distribution of D-AIP in the female mice or total volume consumed during the study period. The data are average from six animals (n = 6). D-AIP, AIP (RGTFEGKF) synthesized using D-amino acids.

Discussion

We have previously shown *in vitro* that a small 8-amino acid peptide (*i.e.*, D-AIP) can (i) specifically "trap" a population of low-order Aβ42 oligomers and render them nontoxic, as well as (ii) suppresses the formation of mature fibrils (18). Using a transgenic *D. melanogaster* model, we have also shown *in vivo* that D-AIP can protect against Aβ42-mediated toxicity in a 28-days longitudinal study (19), which may serve as a novel
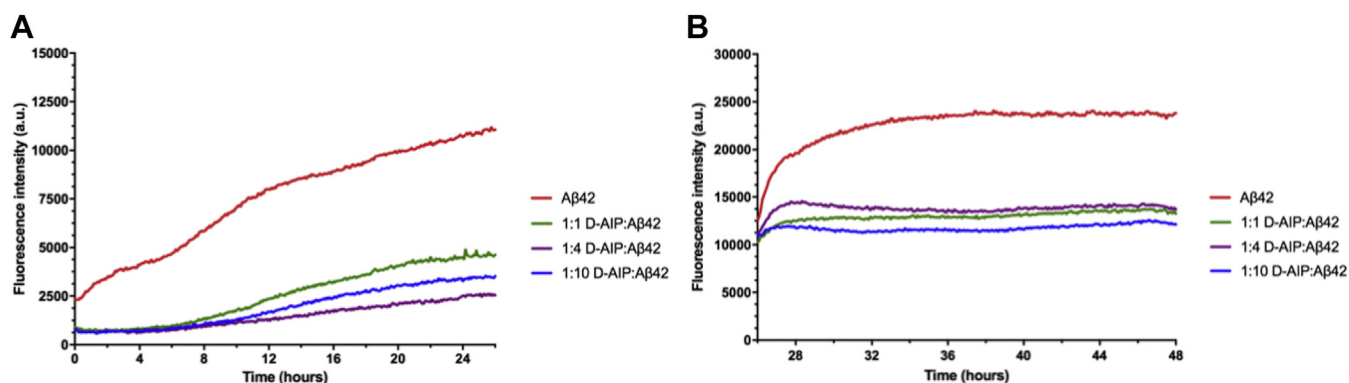
Figure 6. Treatment of freshly dissolved or 24 h preformed aggregates with D-AIP. Freshly monomerized Aβ42 peptide (*A*) and aggregates of Aβ42 (*B*) incubated at room temperature with or without D-AIP at a molar ratio of 1:1, 1:4, and 1:10 (D-AIP:Aβ42), respectively. D-AIP containing Aβ42 showed characteristic stabilization of ThT fluorescence intensity, this suggested the inhibition of Aβ42 aggregation by D-AIP as shown in (*A*). On the other hand, (*B*) revealed that D-AIP prevented secondary Aβ42 nucleation, in contrast to Aβ42 (control) which exhibited a steady increase in ThT fluorescence. Characteristic initial decrease in the ThT fluorescence emission as shown in (*B*) during the first 0.5 h after transfer into the plate reader was because of the samples equilibrating to the incubation temperature. D-AIP, AIP (RGTFEGKF) synthesized using D-amino acids; ThT, thioflavin.

therapeutic strategy to target amyloid pathology in AD (Fig. S4).

To advance the development of our lead D-AIP candidate, the present study examined the metabolic resistance of D-AIP toward proteases and enzymatic activities in mouse plasma, blood, and liver S9 fractions. Under the *ex-vivo* conditions tested (*i.e.*, 24 h at 37 °C), D-AIP appeared to be very stable in the plasma and blood matrices, which likely reflects the enhanced resistance of D-amino acid peptides to proteolysis (20). The inherent instability of L-AIP under similar conditions was expected because the peptides comprised L-amino acids, which are more sensitive to enzymatic degradation (18–20). To assess the potential of D-AIP as an orally administrable therapeutic, our *ex-vivo* testing of D-AIP stability mimicked *in vivo* conditions because esterases, oxidases, and peptidases are actively abundant in biological matrices outside the liver, especially in the blood or plasma. Compared with the time zero control, the decreased signal intensity for D-AIP after 24 h at 37 °C in the liver S9 fractions likely reflected its enzymatic degradation by the D-amino acid oxidase (D-AAO, EC 1.4.3.3), which is associated with oxidative deamination and α-keto acids/ammonia end products in the liver (22–24). Although D-AIP was stable and nontoxic in our *in vivo* fly model (19), the natural ability of the liver to detoxify foreign substances is a desirable effect to avoid any potential long-term accumulation of D-AIP in the human body.

In the present preclinical study, our assessment of D-AIP in male and female WT (C57LB/6) mice progressed from the short-term PK (24 h administration) to its long-term administration (continuous 30-days dose). In the short-term study, D-AIP exhibited favorable PK properties and BBB penetration in both sexes after single oral doses of 10, 30, or 100 mg/kg. D-AIP was well-tolerated at all dosages with no detectable abnormalities in any of the mice before or after termination, and the simplicity and noninvasiveness of oral D-AIP administration was highly advantageous compared with other routes of administration (25). The calculated AUC values, which measured the total systemic exposure of D-AIP across the different doses throughout the 24-h, short-term study, yielded a linear relationship when plotted as a function of D-AIP dosage in both sexes. The calculated maximum concentration values in plasma (C_{max}) as a function of dosage also yielded a linear relationship in both sexes. Because the time at which C_{max} was reached (T_{max}) was either 0.5 or 2 h in all cases, this likely suggests that D-AIP was rapidly absorbed in the intestine and transported to the blood stream for distribution to solid tissues.

The C_{max} values in both sexes as a function of dosage were consistent with the measured V_d in the short-term study. In both female and male mice, the relatively high V_d values across all three doses highlight the propensity of D-AIP to leave the plasma and enter the extravascular compartments of the body, for example, cellular, interstitial, and lymphatic subcompartments as well as a specialized system containing cerebrospinal fluid in the central nervous system. The V_d values also suggest that D-AIP likely has relatively minimal protein-binding properties, which allowed it to leave the protein-rich plasma and distribute into tissues, consequently reducing the plasma half-life of D-AIP as the dose was increased. The relatively low molecular weight of D-AIP (941 Da) may have also supported its passage through endothelia gap junctions of the capillaries into interstitial fluids in the body.

The V_d values for D-AIP indicate that its penetration into brain may likely occur by passive diffusion, that is, movement across cell membranes without the need for energy (26). To avoid labeling D-AIP with traditional radioactive tracers (*e.g.*, 3-H and 14-C), we used label-free MALDI-MSI (27, 28) to detect the relative abundance and spatial distribution of D-AIP in the brain sections of the treated WT mice (*versus* nontreated, PBS-only controls). Taken together, the PK data and MALDI-MSI results support our mechanistic hypothesis that D-AIP entry into the brain occurs by passive diffusion.

In the long-term study, the continuous 30-days dose of D-AIP (at 10 mg/ml in PBS) provided additional evidence of its nonaccumulation in the plasma, which may reflect its minimal
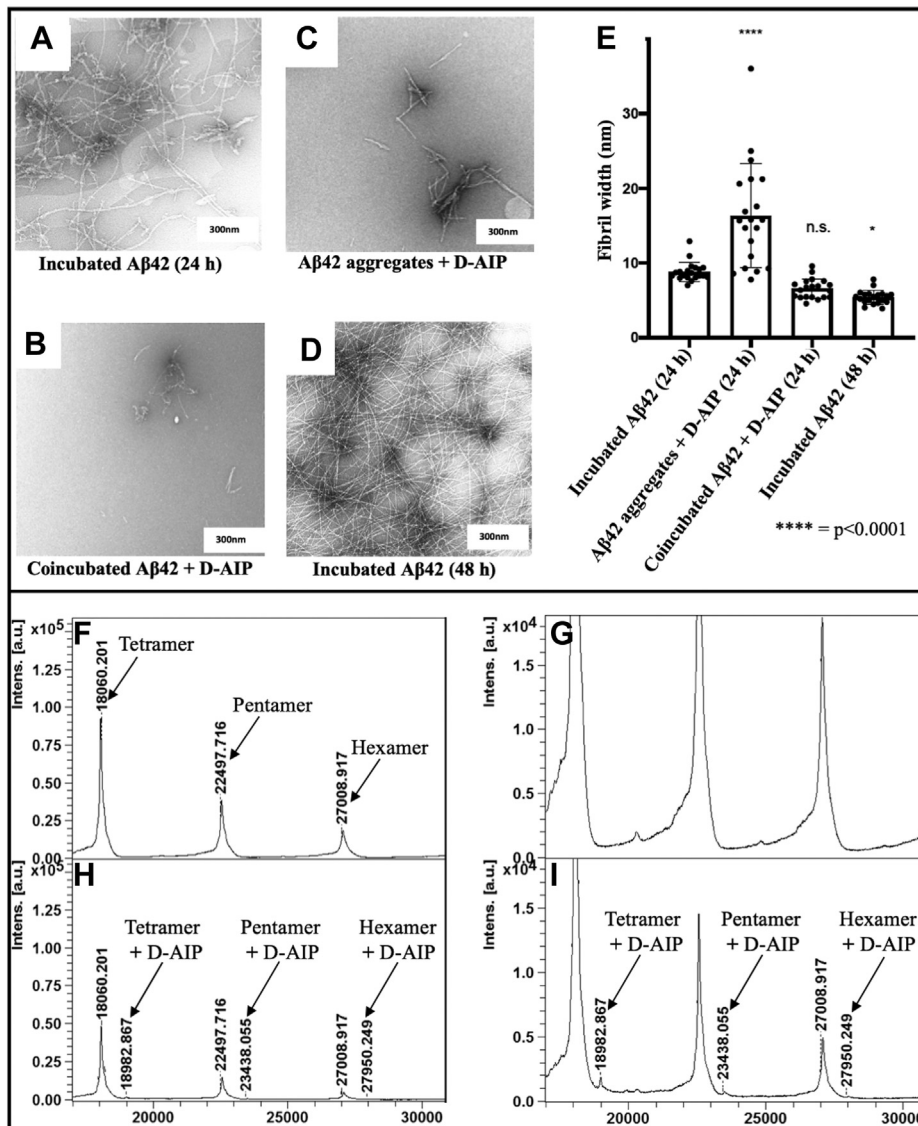
Figure 7. Interactions of D-AIP with Aβ42 aggregates. Transmission electron microscopy (TEM) images of Aβ42 with or without D-AIP and the quantification of the fibril widths. *A*, freshly monomerized Aβ42 incubated for 24 h, (*B*) Aβ42 aggregates coincubated with D-AIP for 24 h, (*C*) freshly monomerized Aβ42 coincubated with D-AIP, (*D*) freshly monomerized Aβ42 incubated for 48 h, (*E*) representative chart for the quantification of fibril widths (Data was analyzed using one-way ANOVA with Dunnett's post-test. n.s. = non-significant, *$p < 0.05$, ****$p < 0.0001$). The lower panels are the MALDI-TOF MS spectrums of residue of (*F*) incubated Aβ42 peptide and its enlarged view (*G*), which revealed only low order oligomers like the tetramers (18,060 *m/z*), pentamers (22,497 *m/z*), and hexamers (27,008 *m/z*) of the Aβ42 peptide. Respective MALDI-TOF MS spectrum (*H*) represents the residue obtained after Aβ42 aggregates were coincubated with D-AIP for 24 h and its enlarged view (*I*). The Aβ42 aggregates treated with 20-fold molar excess of D-AIP led to D-AIP-bound Aβ42 oligomers with representative peaks at 18,982, 23,438, and 27,950 *m/z*. *All incubation conditions were at room temperature. The mass spectrometry spectrums result as shown in (*F*) and (*G*) revealed that in the absence of D-AIP, the incubated Aβ42 alone only showed the masses of the low number oligomers (tetramers, pentamer, and hexamer) respectively. On the contrary, D-AIP interacted with low-order oligomers as shown in (*H*) and (*I*), with an approximate mass increase of about 940 Da in each case that represents that of D-AIP. D-AIP, AIP (RGTFEGKF) synthesized using D-amino acids.

protein-binding property. Once again, D-AIP successfully penetrated the intact BBB in both male and female WT mice as evidenced by the brain concentrations measured. Notably, the sex-based difference in the brain concentrations may relate to the calculated V_d values, which suggested that D-AIP reached a steady state in females considering the similarly close plasma and brain concentrations that were measured in the females.

Building upon our long-term focus on Aβ42 aggregation and toxicity (21) and preliminary analyses of D-AIP (18, 19), the present study provides added insights into the effect of

D-AIP on the three phases of Aβ42 aggregation (*i.e.*, primary nucleation, elongation, and secondary nucleation) (29) as well as fibril proliferation. Based upon the tetramer being the minimal unit required to meet the steric and spatial constraints to bind to the groove of low-order oligomeric forms (2), we hypothesized that in the presence of Aβ42 tetramers, the D-AIP:Aβ42 ratio of 1:4 would efficiently inhibit the immediate aggregation of freshly dissolved Aβ42 peptides targeting *in statu nascendi* produced oligomers (21).

Consistent with our previous molecular modeling and the predicted preference of D-AIP to interact with low-order Aβ42

oligomers such as tetramers (18), the present ThT results showed that the aggregation of freshly monomerized Aβ42 over 24 h was attenuated most effectively using a 1:4 M ratio of D-AIP:Aβ42 (*i.e.*, one D-AIP bound per Aβ42 tetramer). Specifically, the primary nucleation phase (<10 h) was impacted to similar extents at all three ratios tested, whereas the 1:4 ratio was more effective at attenuating the subsequent elongation and secondary nucleation phases between 10 and 24 h. The inhibitory effect of D-AIP on the early aggregation steps is likely because of its binding to tetramers (18) as well as pentamers and hexamers as supported by our present MALDI-TOF data. This finding might also explain why the 1:4 and even higher 1:10 ratio effectively attenuated the subsequent nucleation of preformed Ab42 aggregates between 24 and 48 h.

In the absence of D-AIP, our complementary TEM images revealed that mature, densely packed fibrils were formed after Aβ42 was incubated for 24 h (10 nm diameters) or 48 h (8 nm diameters). The presence of D-AIP impacted the subsequent formation of mature fibrils when preaggregated Aβ42 was incubated from 24 h and 48 h, such that the resultant combination of stunted fibrillar and prefibrillar assemblies exhibited enlarged fibril widths of approximately 18 nm. The significantly increased fibril width suggests that the interaction of D-AIP with preaggregated Aβ42 may be distinct compared with the interaction of D-AIP with freshly monomerized Aβ42.

Together, the biophysical results (complementary ThT and TEM) support a mechanism in which D-AIP specifically targets oligomers (*i.e.*, before larger aggregates are formed) by blocking the inter- and intra-molecular forces required for the formation of proto-fibrils. Our previous molecular modeling (18) had indicated that the protonated N-terminus of D-AIP (Arg1) makes H-bonds to Asp23 in Aβ42, thus interfering with an essential Asp23-Lys28 salt bridge that is required to promote fibril growth (*i.e.*, single Asp23 to Asn substitution within Aβ42 abolishes the ability of D-AIP to inhibit mature fibril formation). On the other hand, D-AIP prevented the secondary nucleation of Aβ42 most effectively at a 10-fold molar excess of Aβ42 (1:10, D-AIP:Aβ42) in the ThT assay, thus implying that D-AIP can also target the higher-order oligomers (*i.e.*, hexamers, octamers, and decamers) that are naturally present in freshly monomerized Aβ42 solutions (21). Thereby, D-AIP is likely affecting the secondary nucleation of Aβ42 (defined as the formation of new nuclei catalyzed by existing fibrils (30)) through its favorable penetration of the glycine (Gly) groove of Aβ42 oligomers. As a result, D-AIP could trap and neutralize accessible neurotoxic oligomers and protofibrils. Overall, the formation of oligomers and fibrils is a step-wise process, involving a rare nucleation event where a susceptible monomeric Aβ form stable aggregates (15). The Aβ deposition phase, which is generally defined as one without clinical symptoms, may already be a reasonably late indicator of a much earlier pathogenic seed formation and propagation that presently escapes detection (16). Therefore, it is advantageous that D-AIP seemingly has a destabilizing effect on seeds either by inhibiting further aggregation or disaggregating them and thus arresting the further growth process of fibrils.

There have been no new Alzheimer drugs approved for almost 20 years (31), with the recent exception of aducanumab (approved by FDA on June 7, 2021). This may be partly because of the complexity of the disease, unmet needs for effective therapeutics hindered by poor PK properties, toxicity, and insufficient drug penetration of the BBB. Although other therapeutic peptides have been designed against the central region of Aβ (32, 33), D-AIP is advantageous in its ability to target the hydrophobic, C-terminal region of Aβ42 (18). Other peptides targeting toxic oligomers or fibrils (*e.g.*, "D3" 12-mer; (33, 34)) have been shown to create larger aggregates in the process (which may elicit negative downstream effects), whereas D-AIP uniquely does not. Therefore, our lead "amyloid trap", D-AIP, provides a novel mechanism of action to trap/neutralize toxic Aβ oligomers, a promising prophylactic strategy to delay and/or prevent the onset of AD. Because low-order Aβ42 oligomers are the major neurotoxic species before Aβ accumulates into the high-order aggregates, which lead to age-related dysfunction (*e.g.*, progressive cognitive decline, reduced immune function, and increased seizures with accelerated cognitive decline; (35–37)), D-AIP may provide an innovative means to increase the efficiency of amyloid removal as toxic Aβ42 oligomers are released from anti-amyloid, antibody-antigen complexes, for example, therapeutic antibody aducanumab (38).

Conclusion

Our preclinical study demonstrates that D-AIP is a promising candidate for subsequent *in vivo* applications because (i) it was stable toward proteolytic degradation in the biological matrices tested and (ii) its favorable pharmacokinetics in WT (C57BL/6) mice suggests it can be orally administered. Moreover, the favorable BBB permeability of D-AIP and its brain region distribution in WT mice overlaps with the key regions impacted by AD pathology. Based upon its ability to attenuate primary and/or secondary Aβ42 nucleation/aggregation events to inhibit mature fibril formation, we anticipate that D-AIP may provide a novel means to prevent and treat early AD pathology. Future studies are warranted to examine the efficacy of D-AIP in transgenic mouse models of AD, overexpressing of APP and/or tau.

Experimental procedures

Peptides

Synthetic AIP (L- or D-amino acids, RGTFEGKF, 940.5 Da) and scrambled AIP (D-amino acids, EFRKFTGG, 940.5 Da) were produced by BioBasic. Freshly prepared AIP peptides were solubilized at 1 mg/ml in deionized water, vortexed, and then sonicated at 37 Hz and 100% power for 10 min at 4 °C. Synthetic Aβ42 peptide was purchased from Bachem and monomerized and solubilized, as described (18). Briefly, the monomerized peptides were dissolved to 1 mg/ml in deionized water supplemented with ammonia to a final concentration of 0.13% (measured pH 9.8). Before experiments, newly

resuspended batches of AIP or Aβ42 peptides were diluted to 0.5 mg/ml in TA50 (0.1% (v/v) trifluoracetic acid: acetonitrile = 50:50) to verify their intact mass by MALDI-MS (Bruker UltrafleXtreme system) and sequence by ESI-MS (Bruker Impact II system).

Ex-vivo *stability study*

Whole mouse blood obtained from healthy C57BL/6 male and female mice (six mice in total) were collected in lithium heparin containing tubes, pooled, and stored at 4 °C before its use. A fraction of the pooled blood was immediately centrifuged at 1500g for 10 min at 4 °C to obtain the plasma. The whole blood and plasma samples were spiked with PBS (as control) or AIP (L-AIP, D-AIP, or sD-AIP, respectively) to make a final concentration of 1 μg/ml and incubated at 37 °C. The initial samples were withdrawn to represent t = 0 before incubation and others were withdrawn 1, 3, and 24 h, respectively. Fresh mouse liver also obtained from C57BL/6 male and female mice were pooled, homogenized in 0.15 M Potassium chloride (KCl), and centrifuged at 9000g. The supernatant represents liver homogenate (S9) fraction, which was mixed with other buffers to formulate the liver S9 mix, as previously described (39). Liver S9 mix were spiked with AIP to make a final concentration of 1 μg/ml (L-AIP, D-AIP, or sD-AIP, respectively) and incubated at 37 °C. Just after the addition of NADPH, 100 μl aliquot which represents t = 0 samples were withdrawn, and others were sampled accordingly at predetermined time points. 400 μl of ice cold MeOH was added to the spiked plasma, blood, or liver S9 fraction respectively, to precipitate the microsomal protein. The samples were then vigorously mixed for 30 s to facilitate extraction and centrifuged for 10 min at 13,000 rpm, the supernatant was subjected to sample clean up by C18 ZipTip (EMD Millipore Corporation), and the eluates were spotted with α-cyano-4-hydroxy cinnamic acid (CHCA) matrix on the ground steel MALDI-TOF target and analyzed with MALDI-TOF MS. Applying the t = 0 peak area as 100%, the intensities of the other time points were compared relatively for interpretation.

Analytical procedure

An internal standard (IS) for the reliable quantification of D-AIP in biological matrices was prepared by dimethylation to produce an analog of D-AIP by using a protocol previously described (40). Standard solutions (1 mg/ml) each of D-AIP and IS were prepared in deionized water and 100% methanol respectively. One hundred microliters of IS working solution was prepared at 50 ng/ml added to 25 μl of the sample (plasma or brain homogenate). The sample was vortexed for approximately 5 s and let stand for 10 min, then centrifuged at 16,000g for 10 min. The supernatant was transferred to a 13 × 100 polypropylene tube and evaporated to dryness at 50 °C under gentle stream of nitrogen. The dry extract was resuspended with 40 μl of 0.1% (v/v) formic acid (Sigma Aldrich) in deionized water and transferred to an injection vial for analysis.

Instruments

Thermo Scientific TSQ Quantiva Triple Quadrupole mass spectrometer was interfaced with the Thermo Scientific UltiMate 3000 XRS UHPLC system using a pneumatic-assisted heated electrospray ion source. Data acquisition and analysis were performed using Xcalibur 4.0.

Chromatographic conditions

Gradient elution was used with a Thermo Scientific BioBasic-8 column (100 × 2 mm I.D. 5 μm) operating at 40 °C. The initial mobile phase condition consisted of 0.1% formic acid in acetonitrile and 0.1% formic acid in deionized water at a ratio of 5:95, respectively, and this ration was maintained for 1 min. A linear gradient was applied from 1 to 5 min up to a ratio of 50:50 and maintained for 1 min. At 6.1 min, the mobile phase composition was reverted to 5:95, and the column was allowed to equilibrate for 7.9 min for a total run time of 14 min. The D-AIP and IS eluted at 4.7 and 4.8 min respectively at a fixed flow rate of 0.2 ml/min. The eluent was diverted to waste for the first minute and last 6 min. The extracted sample (5 μl) was injected, and the acquisition time was set to 14 min.

Mass spectrometric conditions

The mass spectrometer was interfaced with ultra-HPLC system using a pneumatic-assisted heated electrospray ion source with detection in positive ion mode using multiple ion monitoring. For proper optimization of the mass spectrometer, standard solutions of D-AIP and IS were infused. The obtained source parameters were 50 and 15 arbitrary units, respectively, while using nitrogen for the sheath and auxiliary gases. The HESI electrode was set to 3500 V, and capillary and vaporizer temperature were both set to 300 °C, respectively. The MS/MS parameters were optimized using the doubly charged species. Argon was used as collision gas at a pressure of 2.5 mTorr. The precursor-ion reaction for D-AIP were set to $471.4 \rightarrow [591.3 + 648.3]$, and for the IS, the multiple ion monitoring transitions were set to $499.4 \rightarrow [425.8 + 468.8 + 476.8]$.

Analytical quantification

Standard solution of D-AIP (1 mg/ml) was diluted in various volumes of deionized water to obtain a series of standard working solutions. Calibration standards were prepared by fortifying the mouse plasma and mouse brain homogenate with the standard working solutions at 10% (v/v) to enable analytical concentration range of 1.00 to 1000 ng/ml. The method is linear using a linear regression weighted $1/x$ analysis, and a value of $R^2 \geq 0.9979$ was obtained for plasma and $R^2 \geq 0.9991$ for brain homogenate. The samples were injected in duplicate with the calculated in each case, and concentrations were processed from the equation obtained from the respective calibration curves using Xcalibur 4.0 software.

AIP possesses favorable anti-amyloid properties

Pharmacokinetics

Animal care and all animal experiments were undertaken with federal guidelines and approval of the Institutional Animal Ethical Committee of McGill University (Protocol Application Number: 2017-7880), and adequate measures were taken to minimize pain or discomfort. C57BL/6 mice were purchased from Charles River laboratories, a total of 144 healthy (7–9 weeks old) male and female (20–25 g) were grouped accordingly and housed in polycarbonate cages, (three mice per cage per sex) in air-conditioned rooms with a 12 h light/dark cycle. The animals were allowed unlimited access to drinking water and standard mouse chow during the study. The animals (n = 3) were orally dosed with D-AIP using an oral gavage at 10, 30, and 100 mg/kg respectively prepared in PBS. The animals were euthanized with 5% isoflurane followed by cervical dislocation. Blood collection (approximately 500 μl each) in lithium heparin containing tubes (BD microtainer) were by intracardiac puncture at 0.5, 2, 4, 6, 8, 12, and 24 h postdose. Control animals were orally dosed with PBS and euthanized, as described above, at 3 h postadministration. All blood samples were centrifuged at $1500g$ for 10 min at 4 °C and aliquots of plasma (approximately 0.5 ml) were immediately kept on dry ice and later stored at −80 °C before analysis. The brains were surgically removed from all animals and immediately frozen on dry ice before storage at −80 °C. Pharmacokinetic parameters AUC, C_{max}, T_{max}, elimination rate constant (λz), $t_{1/2}$, CL/F, V_d, and MRT were calculated using PKSolver, a freely available menu-driven add-in program for Microsoft Excel written in Visual Basic for Applications, for solving problems in PK.

Long-term administration of D-AIP

Animal care and all animal experiments were undertaken with federal guidelines and approval of the Institutional Animal Ethical Committee of McGill University (Protocol Application Number: 2017-7880) and adequate measures were taken to minimize pain or discomfort. C57BL/6 mice were purchased from Charles River laboratories, a total of 24 healthy (8 weeks old) male and female were grouped accordingly and housed in polycarbonate cages, (three mice per cage per sex) in air-conditioned rooms with a 12 h light/dark cycle. The animals were allowed unlimited oral access to D-AIP dissolved in PBS at a concentration of 10 mg/ml and standard mouse chow for 30 days. In parallel, control animals were provided with PBS for the same study time. The animals were euthanized with 5% isoflurane followed by cervical dislocation after the study. Blood collection (approximately 500 μl each) in lithium heparin containing tubes (BD microtainer) was by intracardiac puncture.

Matrix assisted laser desorption ionization mass spectrometry imaging

For the MALDI imaging study, additional four mice (two males and two females) were orally dosed either with PBS or D-AIP (10 mg/kg) and sacrificed 4 h postadministration (at the time maximum concentration was reached in the lowest dose),

as described above. The frozen brains were stored at −80 °C until needed for analysis. Serial sagittal brain sections (10 μm thick) obtained using a cryostat (Leica Microsystems CM1100), were thaw mounted onto an indium tin oxide-coated glass slide (Bruker). The glass slides were removed from deep freeze and immediately transferred to a vacuum desiccator. After 12 h desiccation time, the slides were scanned using a flatbed scanner (HP LaserJet 3055). The CHCA matrix (10 mg/ml) was prepared in 50% acetonitrile containing 0.1% trifluoroacetic acid. The matrix solution was sonicated for 10 min and centrifuged at 10,000 rpm for 10 min before transfer to the ImagePrep (Bruker Daltonics). An automatic spraying device that deposits matrix solution onto the tissue in a consistent manner under controlled conditions, as previously described ([41]). A standard solution of D-AIP (1 μg/ml) was analyzed using MALDI TOF MS operated both at reflectron and MALDI MS/MS (LIFT) modes respectively with the aid of the UltrafleXtreme MALDI TOF/TOF 2 KHz smartbeam laser (Bruker Daltonics) and FlexControl acquisition software ran in positive ion mode. The instrument was calibrated using standard peptide mix spotted with CHCA matrix on the ground steel target (Bruker Daltonics) for 500 to 1500 m/z. Each spectrum was acquired from 500 laser shots. The LIFT experiments were performed using a method optimized for the drug by specific tuning of the timing of the LIFT cell and of the precursor ion selector. The LIFT method was calibrated with peptide calibration standards and also a standard solution of D-AIP, as mentioned above. The tissue sections were imaged with spatial resolution 50 μm. The MALDI images were processed using the FlexImaging 4.0 software (Bruker Daltonics).

Thioflavin T assay

Freshly monomerized synthetic Aβ42 peptide was dissolved, as previously described above. The final concentration was verified by spectrophotometry, using a Synergy H1 multimode microplate reader (BioTek; $\varepsilon_{280} = 1490$ M^{-1} cm^{-1} for Aβ42) and adjusted if required by addition of 0.5% (v/v) ammonia water. ThT solution was diluted in PBS (20 mM Na_2HPO_4 and 150 mM NaCl, pH 7.4) in a threefold molar excess to the desired Aβ concentration, before Aβ42 with or without D-AIP were added as well, making up a final volume of 300 μl. The measurements were performed in triplicates, for which 100 μl of the solution were transferred per well on a black Nunc Microwell 96-Well Optical-Bottom Plate (ThermoFisher Scientific). The controls were included for each peptide concentration, containing the threefold concentration of ThT but no peptide. The plate was sealed using protective foil to avoid evaporation in the course of the measurement. Fluorescence was measured at 485 nm upon excitation at of 450 nm every 5 min for a total of 40 h, at room temperature. The control values were ultimately subtracted at each time point for normalization.

Transmission electron microscopy

Aβ peptides were dissolved to 40 μM and incubated for 24 h at room temperature with or without D-AIP at a ratio of 1:20

(Aβ42:AIP). After 24 h incubation, a portion without D-AIP was then added with appropriate amount of D-AIP (1:20) and further incubated for another 24 h. Aliquots (4 μl) of matured peptide solutions in all instances were applied to glow-discharged carbon-coated copper grids (Electron Microscopy Sciences, EMS300-Cu) and negatively stained with 2% aqueous uranyl acetate, as described (42). The data was collected on a FEI Tecnai G2 Spirit Twin electron microscope operated at 120 kV with a Gatan Ultrascan 4000 CCD camera at the Facility for Electron Microscopy Research at McGill University. In an attempt to further characterize the structural state of the Aβ42 aggregates interacting with D-AIP, immediately after spotting on the glow-discharged carbon-coated copper grids of the TEM in both experiments (*i.e.*, coincubation of freshly prepared Aβ42 with D-AIP and preformed aggregates with D-AIP, respectively, as earlier described), the rest of the samples were centrifuged at a speed of 13,000 rpm for 10 min, and residue spotted with sDHB matrix on the polished steel MALDI-TOF target for mass acquisition using linear positive mode of the MALDI-TOF MS. The spectrums were acquired using the MALDI-TOF MS to observe the current state of the incubated Aβ42 with or without D-AIP.

Data availability

The authors confirm that the data supporting the findings of this study are available within the article and its supplementary materials.

Conflict of interest—The authors declare that they have no conflict of interest with the contents of this article.

Abbreviations—The abbreviations used are: Aβ, amyloid-beta; AD, Alzheimer's disease; AIP, Aβ42-oligomer interacting peptide; APP, amyloid precursor protein; AUC, area-under the curve; BBB, blood brain barrier; CHCA, α-cyano-4-hydroxy cinnamic acid; CL/F, apparent total clearance from plasma after oral administration; C_{max}, maximum concentration reached; D-AIP, AIP (RGTFEGKF) synthesized using D-amino acids; IS, internal standard; L-AIP, AIP (RGTFEGKF) synthesized using L-amino acids; MRT, mean residence time; MSI, mass spectrometry imaging; PK, pharmacokinetics; sD-AIP, scrambled version of D-AIP (EFRKFTGG); $t_{1/2}$, elimination half-life; TEM, transmission electron microscopy; T_{max}, time at which maximum concentration is reached; ThT, thioflavin T; V_d, apparent volume of distribution.

References

1. Hardy, J., Bogdanovic, N., Winblad, B., Portelius, E., Andreasen, N., Cedazo-Minguez, A., and Zetterberg, H. (2014) Pathways to Alzheimer's disease. *J. Intern. Med.* **275**, 296–303
2. Selkoe, D. J., and Hardy, J. (2016) The amyloid hypothesis of Alzheimer's disease at 25 years. *EMBO Mol. Med.* **8**, 595–608
3. Yan, R., and Vassar, R. (2014) Targeting the β secretase BACE1 for Alzheimer's disease therapy. *Lancet Neurol.* **13**, 319–329
4. De Strooper, B., and Annaert, W. (2010) Novel research horizons for presenilins and γ-secretases in cell biology and disease. *Annu. Rev. Cell Dev. Biol.* **26**, 235–260
5. Glabe, C. G., and Kayed, R. (2006) Common structure and toxic function of amyloid oligomers implies a common mechanism of pathogenesis. *Neurology* **66**, S74–S78
6. Walsh, D. M., Klyubin, I., Fadeeva, J. V., Cullen, W. K., Anwyl, R., Wolfe, M. S., Rowan, M. J., and Selkoe, D. J. (2002) Naturally secreted oligomers of amyloid beta protein potently inhibit hippocampal long-term potentiation *in vivo*. *Nature* **416**, 535–539
7. Zhao, L. N., Long, H., Mu, Y., and Chew, L. Y. (2012) The toxicity of amyloid β oligomers. *Int. J. Mol. Sci.* **13**, 7303–7327
8. Haass, C., and Selkoe, D. J. (2007) Soluble protein oligomers in neurodegeneration: Lessons from the Alzheimer's amyloid β-peptide. *Nat. Rev. Mol. Cell Biol.* **8**, 101–112
9. Long, J. M., and Holtzman, D. M. (2019) Alzheimer disease: An update on pathobiology and treatment strategies. *Cell* **179**, 312–339
10. Mawuenyega, K. G., Sigurdson, W., Ovod, V., Munsell, L., Kasten, T., Morris, J. C., Yarasheski, K. E., and Bateman, R. J. (2010) Decreased clearance of CNS beta-amyloid in Alzheimer's disease. *Science* **330**, 1774
11. Jack, C. R., Jr., Knopman, D. S., Weigand, S. D., Wiste, H. J., Vemuri, P., Lowe, V., Kantarci, K., Gunter, J. L., Senjem, M. L., Ivnik, R. J., Roberts, R. O., Rocca, W. A., Boeve, B. F., and Petersen, R. C. (2012) An operational approach to National Institute on Aging–Alzheimer's Association criteria for preclinical Alzheimer disease. *Ann. Neurol.* **71**, 765–775
12. Liebsch, F., Kulic, L., Teunissen, C., Shobo, A., Ulku, I., Engelschalt, V., Hancock, M. A., van der Flier, W. M., Kunach, P., Rosa-Neto, P., Scheltens, P., Poirier, J., Saftig, P., Bateman, R. J., Breitner, J., *et al.* (2019) Aβ34 is a BACE1-derived degradation intermediate associated with amyloid clearance and Alzheimer's disease progression. *Nat. Commun.* **10**, 2240
13. Langer, F., Eisele, Y. S., Fritschi, S. K., Staufenbiel, M., Walker, L. C., and Jucker, M. (2011) Soluble Aβ seeds are potent inducers of cerebral β-amyloid deposition. *J. Neurosci.* **31**, 14488
14. Villemagne, V. L., Doré, V., Burnham, S. C., Masters, C. L., and Rowe, C. C. (2018) Imaging tau and amyloid-β proteinopathies in Alzheimer disease and other conditions. *Nat. Rev. Neurol.* **14**, 225–236
15. Jarrett, J. T., and Lansbury, P. T., Jr. (1993) Seeding "one-dimensional crystallization" of amyloid: A pathogenic mechanism in Alzheimer's disease and scrapie? *Cell* **73**, 1055–1058
16. Uhlmann, R. E., Rother, C., Rasmussen, J., Schelle, J., Bergmann, C., Ullrich Gavilanes, E. M., Fritschi, S. K., Buehler, A., Baumann, F., Skodras, A., Al-Shaana, R., Beschorner, N., Ye, L., Kaeser, S. A., Obermüller, U., *et al.* (2020) Acute targeting of pre-amyloid seeds in transgenic mice reduces Alzheimer-like pathology later in life. *Nat. Neurosci.* **23**, 1580–1588
17. Sato, T., Kienlen-Campard, P., Ahmed, M., Liu, W., Li, H., Elliott, J. I., Aimoto, S., Constantinescu, S. N., Octave, J. N., and Smith, S. O. (2006) Inhibitors of amyloid toxicity based on beta-sheet packing of Abeta40 and Abeta42. *Biochemistry* **45**, 5503–5516

18. Barucker, C., Bittner, H. J., Chang, P. K., Cameron, S., Hancock, M. A., Liebsch, F., Hossain, S., Harmeier, A., Shaw, H., Charron, F. M., Gensler, M., Dembny, P., Zhuang, W., Schmitz, D., Rabe, J. P., *et al.* (2015) Aβ42-oligomer interacting peptide (AIP) neutralizes toxic amyloid-β42 species and protects synaptic structure and function. *Sci. Rep.* **5**, 15410

19. Zhong, Y., Shobo, A., Hancock, M. A., and Multhaup, G. (2019) Label-free distribution of anti-amyloid D-AIP in Drosophila melanogaster: Prevention of Aβ42-induced toxicity without side effects in transgenic flies. *J. Neurochem.* **150**, 74–87

20. Feng, Z., and Xu, B. (2016) Inspiration from the mirror: D-amino acid containing peptides in biomedical approaches. *Biomol. Concepts* **7**, 179–187

21. Harmeier, A., Wozny, C., Rost, B. R., Munter, L.-M., Hua, H., Georgiev, O., Beyermann, M., Hildebrand, P. W., Weise, C., Schaffner, W., Schmitz, D., and Multhaup, G. (2009) Role of amyloid-β glycine 33 in oligomerization, toxicity, and neuronal plasticity. *J. Neurosci.* **29**, 7582

22. D'Aniello, A., D'Onofrio, G., Pischetola, M., D'Aniello, G., Vetere, A., Petrucelli, L., and Fisher, G. H. (1993) Biological role of D-amino acid oxidase and D-aspartate oxidase. Effects of D-amino acids. *J. Biol. Chem.* **268**, 26941–26949

23. Krebs, H. A. (1935) Metabolism of amino-acids: Deamination of amino-acids. *Biochem. J.* **29**, 1620–1644

24. Ohide, H., Miyoshi, Y., Maruyama, R., Hamase, K., and Konno, R. (2011) D-amino acid metabolism in mammals: Biosynthesis, degradation and analytical aspects of the metabolic study. *J. Chromatogr. B Analyt. Technol. Biomed. Life Sci.* **879**, 3162–3168

25. Surnar, B., Kamran, M. Z., Shah, A. S., Basu, U., Kolishetti, N., Deo, S., Jayaweera, D. T., Daunert, S., and Dhar, S. (2019) Orally administrable therapeutic synthetic nanoparticle for zika virus. *ACS Nano* **13**, 11034–11048

26. Pignatello, R. (2013) 1 - Biological membranes and their role in physio-pathological conditions. In: Pignatello, R., ed. *Woodhead Publishing Series in Biomedicine, Drug-Biomembrane Interaction Studies*, Woodhead Publishing, Sawston, UK: 1–46

27. Prideaux, B., and Stoeckli, M. (2012) Mass spectrometry imaging for drug distribution studies. *J. Proteomics* **75**, 4999–5013

28. Römpp, A., and Karst, U. (2015) Current trends in mass spectrometry imaging. *Anal. Bioanal. Chem.* **407**, 2023–2025

29. Thacker, D., Sanagavarapu, K., Frohm, B., Meisl, G., Knowles, T. P. J., and Linse, S. (2020) The role of fibril structure and surface hydrophobicity in secondary nucleation of amyloid fibrils. *Proc. Natl. Acad. Sci. U. S. A.* **117**, 25272

30. Dobson, C. M., Knowles, T. P. J., and Vendruscolo, M. (2020) The amyloid phenomenon and its significance in biology and medicine. *Cold Spring Harb. Perspect. Biol.* **12**, a033878

31. Cummings, J., Lee, G., Ritter, A., Sabbagh, M., and Zhong, K. (2019) Alzheimer's disease drug development pipeline: 2019. *Alzheimers Dement. (N. Y.)* **5**, 272–293

32. Mehrazma, B., Opare, S., Petoyan, A., and Rauk, A. (2018) D-amino acid pseudopeptides as potential amyloid-beta aggregation inhibitors. *Molecules* **23**, 2387

33. Jagota, S., and Rajadas, J. (2013) Synthesis of d-amino acid peptides and their effect on beta-amyloid aggregation and toxicity in transgenic Caenorhabditis elegans. *Med. Chem. Res.* **22**, 3991–4000

34. Aileen Funke, S., van Groen, T., Kadish, I., Bartnik, D., Nagel-Steger, L., Brener, O., Sehl, T., Batra-Safferling, R., Moriscot, C., Schoehn, G., Horn, A. H., Müller-Schiffmann, A., Korth, C., Sticht, H., and Willbold, D. (2010) Oral treatment with the d-enantiomeric peptide D3 improves the pathology and behavior of Alzheimer's disease transgenic mice. *ACS Chem. Neurosci.* **1**, 639–648

35. Vossel, K. A., Tartaglia, M. C., Nygaard, H. B., Zeman, A. Z., and Miller, B. L. (2017) Epileptic activity in Alzheimer's disease: Causes and clinical relevance. *Lancet Neurol.* **16**, 311–322

36. Erickson, M. A., and Banks, W. A. (2013) Blood-brain barrier dysfunction as a cause and consequence of Alzheimer's disease. *J. Cereb. Blood Flow Metab.* **33**, 1500–1513

37. Erickson, M. A., and Banks, W. A. (2019) Age-associated changes in the immune system and blood-brain barrier functions. *Int. J. Mol. Sci.* **20**, 1632

38. Sevigny, J., Chiao, P., Bussière, T., Weinreb, P. H., Williams, L., Maier, M., Dunstan, R., Salloway, S., Chen, T., Ling, Y., O'Gorman, J., Qian, F., Arastu, M., Li, M., Chollate, S., *et al.* (2016) The antibody aducanumab reduces Aβ plaques in Alzheimer's disease. *Nature* **537**, 50–56

39. Kolrep, F., Rein, K., Lampen, A., and Hessel-Pras, S. (2017) Metabolism of okadaic acid by NADPH-dependent enzymes present in human or rat liver S9 fractions results in different toxic effects. *Toxicol. In Vitro* **42**, 161–170

40. Boersema, P. J., Raijmakers, R., Lemeer, S., Mohammed, S., and Heck, A. J. (2009) Multiplex peptide stable isotope dimethyl labeling for quantitative proteomics. *Nat. Protoc.* **4**, 484–494

41. Shobo, A., Bratkowska, D., Baijnath, S., Naiker, S., Bester, L. A., Singh, S. D., Maguire, G. E., Kruger, H. G., and Govender, T. (2015) Visualization of time-dependent distribution of rifampicin in rat brain using MALDI MSI and quantitative LCMS/MS. *Assay Drug Dev. Technol.* **13**, 277–284

42. Scarff, C. A., Fuller, M. J. G., Thompson, R. F., and Iadanza, M. G. (2018) Variations on negative stain electron microscopy methods: Tools for tackling challenging systems. *J. Vis. Exp.* https://doi.org/10.3791/57199